Available online at www.sciencedirect.com

ScienceDirect

Procedia Structural Integrity 18 (2019) 223–230

Structural Integrity Procedia

www.elsevier.com/locate/procedia

25th International Conference on Fracture and Structural Integrity

Design and characterization of linear shape memory alloy actuator with modular stroke

Girolamo Costanza[a]*, Neyara Radwan[b,c], Maria Elisa Tata[d], Emanuele Varone[a]

[a] *Industrial Engineering Department,University of Rome Tor Vergata, Via del Politecnico 1, 00133 Rome, Italy*
[b] *Faculty of Economics & Administration, King AbdulazizUniversity, Jedda, Saudi Arabia*
[c] *Mechanical Department,Faculty of Engineering, Suez Canal University, Egypt*
[d] *Civil Engineering and Computer Science Department, University of Rome Tor Vergata, Via del Politecnico 1, 00133 Rome, Italy*

Abstract

In this work a novel actuation system based on NiTi shape memory springs has been designed and characterized in a small-scale prototype to permit setting of the right aperture and its modulation when necessary. The manufactured prototype exploits an actuator in the antagonist configuration. In particular, the aim has been focused on the modulation of the stroke by the activation of Shape Memory Alloy (SMA) actuators. SMA springs of 15 turns and 7.5 mm average diameter are the optimal solution relatively to force and stroke required from the system. One of the possible applications of such actuator is in the field of solar reactors in which one of the main problem is to keep constant temperature into the reactor in order to allow a continuous and efficient transformation, from sunrise to sunset.

© 2019 The Authors. Published by Elsevier B.V.
Peer-review under responsibility of the Gruppo Italiano Frattura (IGF) ExCo.

Keywords: Shape Memory Alloy, linear actuator, modular stroke, solar reactor.

1. Introduction

Shape memory alloys are a class of functional materials able to recover the preset shape just upon heating above a critical transformation temperature (Costanza et al. (2016)). Thanks to this ability they can be exploited as sensor, transducers or actuators for example in solar sailing, as testified by the published works: Boschetto et al. (2019), Costanza et al. (2018), Costanza et al. (2017). In SMA-based actuators one of the main problem regards the difficulty

* Corresponding author. Tel.: +39 06 72597185; fax: +39 06 2021351
E-mail address: costanza@ing.uniroma2.it

2452-3216 © 2019 The Authors. Published by Elsevier B.V.
Peer-review under responsibility of the Gruppo Italiano Frattura (IGF) ExCo.
10.1016/j.prostr.2019.08.157

in the modulation of the stroke when small adjustments are required. The main purpose of this work is to design and manufacture a novel system of variable aperture which allows to set the right aperture size. It could be employed, for example, in the field of solar reactor according to the value of irradiance during the day. In the proposed prototype the aperture is adjusted by means of a SMA actuator system in antagonist configuration. High activation forces, compactness of the solution, possibility to manage the stroke, durability and reliability of the actuators are the main advantages of the SMA springs proposed in comparison with standard activation systems. SMA wires in linear configuration are not considered, both for activation and antagonist configuration, due to the following drawbacks: low force, huge wire's length, drift of the wire and low stability of the shape memory effect.

Solar reactors are based on a chemical reaction chamber which collects, through an aperture, the concentrated solar energy in order to reach the high temperature required for the endothermic reactions. However, there is a major challenge concerning the maintenance of semi-constant high temperatures inside the solar reactor. Temperature changes are ascribable to the incident solar radiation fluctuation, depending on the position of the sun in the sky and on the weather conditions as illustrated by Ophoff et al. (2017). These systems can be classified in two categories: solar direct reactors and solar indirect ones. An example of solar indirect irradiated reactor was designed by Kräupl et al. (2006), conceived as a fixed aperture reactor which consists of two cavities in series. The upper one acts as a solar absorber, whereas the lower one is employed as a reaction chamber containing a ZnO/C packed bed. The ZnO reduction reaction proceeds endothermic at above 1300 K and the reactor is used for Zn production from ZnO reduction. Heat transfer to the reactor wall is dominated by thermal radiation. At temperatures of above 1500 K, the rate of irradiative heat transfer is much higher than the conductive heat transfer through the insulation. Therefore radiation heat transfer is the dominant mechanism in this reactor. An example of solar direct - irradiated reactor is the solar reactor designed by Z'Graggen et al. (2006) employed for steam-gasification of petcock. The reactor is a cavity receiver and the reaction chamber is directly exposed to the concentrated solar radiation. The main advantage of the solar indirect - irradiated reactor is the removal of the products deposited on the quartz window. The disadvantage is the limited conversion efficiency due to the heat transmission through the separation. For this reason in direct solar system it is possible to achieve higher temperature and conversion rate. These all-solar reactors have fixed aperture and are all subjected to the same natural fluctuation of the incoming solar energy. The main problem is that fluctuations in solar energy radiation prevents to achieve stable and high production process, reducing the efficiency of the thermochemical processes. This phenomenon can be ascribable to the aperture size, kept constant during the change of incoming solar flux levels from sunrise to sunset. State of the art on solar reactor technology shows that an increasing attention is given to the optimal reactor design to achieve steady state efficiency, as reported in Ophoff et al. (2017).

A few techniques have been found in literature to accommodate the instabilities of incoming solar radiation. One of the widely used methods is the mass flow adjustment of the feedstock. This method is widely employed in the chemical industry for traditional processes. In the case of controlled solar reactor temperature the technique is based on the flow rates control according to the incoming solar radiation. Hathaway et al. (2016) studied the isothermal ceria-based solar redox cycle for continuous fuel production in a solar reactor. However, change of mass flow rate modifies the flow pattern inside solar reactors, generating problems in some cases. For example, solar methane cracking requires a particular flow pattern inside the solar reactor. Another method to keep constant temperature is to focus and defocus heliostats using two-axial movement. Heliostat focus/defocus technique is based on the use of heliostat movement in two directions, e.g. upward and downward. The reflective surface of the mirror is kept perpendicular to the bisector of the angle between the directions of the sun and the target as seen from the mirror. In almost every case, the target is stationary relatively to the heliostat, so the light is reflected to a fixed direction. However, to accommodate transient nature of the incoming solar radiation, the heliostats could be focused and defocused, as implemented by Besarati et al. (2014). These traditional methods used to control solar reactor temperature have significant drawbacks. For example, focusing/defocusing heliostats leads to insufficient use of the available energy and is critical due to the high costs. Meanwhile, mass flow adjustment of feedstock modifies the flow pattern inside the reactor and it could be a problem if specific flows are required to be maintained.

2. Materials and methods

The selection of the material for the actuation system is fundamental in order to achieve the best performance in terms of flexibility, force and stroke of the device. The opening of the system, composed by two covers, is due to the activation of the SMA springs guided in their stroke by ceramic guides. The shape recovery based on the thermoelastic

martensitic transformation occurring in such kind of alloys and the characteristic transformation temperatures are function of the composition of the alloy and of the thermal and mechanical history of the material as demonstrated by Costanza et al. (2014). Typical transformation temperatures of NiTi SMA are 65 °C (alloy H) and 95 °C (alloy M) according to the nomenclature used by the supplier of the alloys (Memory Metalle GmbH). Usually employed as sensor, sensor/actuators or only actuators, shape memory alloys are stable for high number of activation cycles if properly designed (Costanza et al. (2010)). As active material, commercial wires of 0.4, 0.6 and 0.8 mm diameter have been identified and selected. In the design of an actuator based on shape memory alloy spring the selection is driven by the optimal compromise between force and stroke. Higher diameter's wire allows greater force but the drawback is shorter stroke. In the proposed application wire of 0.8 mm diameter (alloy M, 95 °C activation temperature) has been employed for the greater force available during the activation. Wires of 0.4 and 0.6 mm diameter have been discarded due to the unsatisfactory force while diameters greater than 0.8 mm are not considered for the lower stroke. For the covers PMMA has been selected for its lightness and workability to build up the lab-scale prototype. For the manufacturing of the spring the wire of 0.8 mm diameter has been turned around a screw of known diameter and the extremities have been fixed at the ends, as shown in Fig. 1. Two commercial steel screws have been employed for this task, allowing 7.6 mm of average diameter and 4.1 mm helical pitch the first one while 6.6 mm average diameter and 3.8 mm helical pitch the second one.

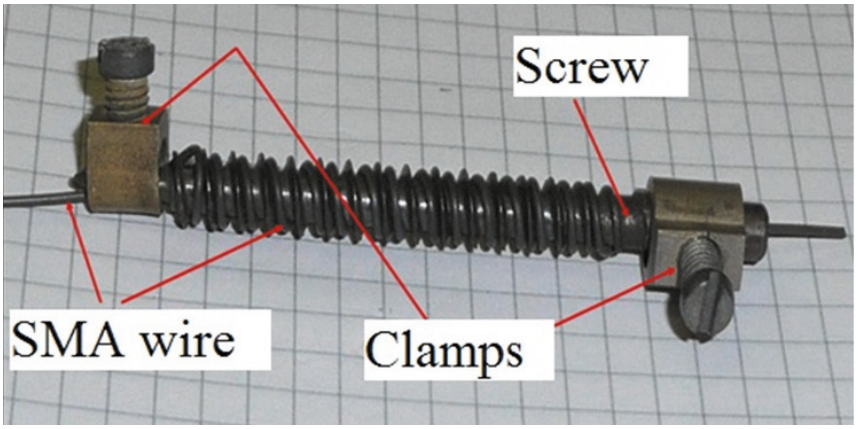

Fig. 1. Manufacture of a SMA spring by means of wire and screw.

Thereafter, to set the shape, different thermal treatments, called shape-setting, have been tested on the spring in order to ensure the recovery of the desired shape when activated. Among the different combinations of temperature and time the best result for the shape setting consists in heating up to 500 °C the spring turned around the screw in the oven, maintaining at this temperature for 10 minutes followed by quenching in cold water (Wang et al. (2002)). After this thermal treatment, compressing in cold condition the spring is able to recover the preset helical shape just upon heating above the activation temperature (95 °C). In this work a lot of springs with different geometrical parameters have been considered by changing the number of turns of the wire in the manufacturing, as reported in Table 1. The selection of the number of turns has been driven by the elastic constant required to the spring, the force and the overall length of the spring. The activation experiments have been aimed to define the optimum among these springs in terms of stroke and the force applied during the activation.

Table 1. Different types of spring manufactured depending on the number of turns, total length, helical pitch and average diameter.

	Spring (a)	Spring (b)	Spring (c)	Spring (d)	Spring (e)
Number of turns	15	13	10	13	16
Total length (mm)	61	53	41	51	60
Helical pitch (mm)	4.1	4.1	4.1	3.8	3.8
Average diameter (mm)	7.6	7.6	7.6	6.6	6.6

Figure 2 shows a spring of 10 turns and 7.6 mm average diameter which if compressed has initial length of 28 mm while after heating reaches the length of 41 mm.

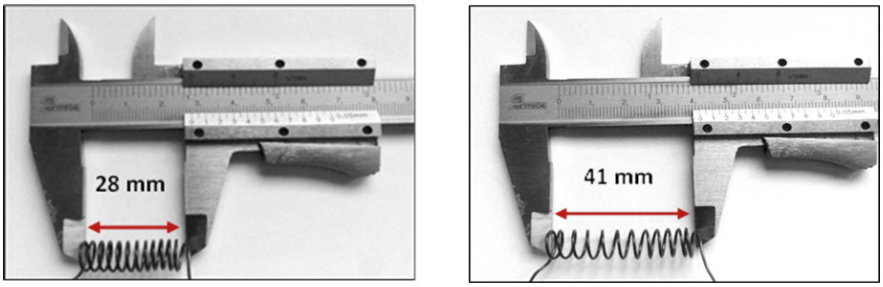

Fig. 2. SMA spring in two different configurations: on the left “compressed spring“, on the right spring with its “memorized length”.

3. Results and discussion

The main parameters, which have been taken into account in this work are the overall length of the spring, the number of turns, the average diameter and the pitch. In the first step of the work the characterization of the spring has been performed in order to determine the value of the stiffness and the elastic constant of each spring. All the springs, both in martensitic and austenitic phase, have been characterized measuring the force by means of a load cell at each corresponding length. To characterize the spring in the austenitic condition, it has been activated by an electrical power supply linking the end of the spring with clamps. Fig. 3 shows the process in the austenitic phase. In Table 2 the experimental elastic constant “k” are reported.

Table 2. Different values of experimental elastic constant for different types of springs.

Spring (experimental)	k martensite (N/m)	k austenite (N/m)
13 Turns, Diameter 6.6 mm	225.5	366.2
13 Turns, Diameter 7.6 mm	168.5	235.5
15 Turns, Diameter 7.6 mm	147.1	216.7

Fig. 3. Characterization of the spring during the compression test.

As reported in Table 2, in the comparison with the same diameter, springs with higher number of turns show lower force. For instance, comparing the spring with the same number of turns, the spring with average diameter 6.6 mm shows higher force during the activation and can't be considered suitable for our purpose due to the higher stiffness. The spring with 15 turns and average diameter of 7.6 mm has been selected because in the prototype tests showed the optimal stroke.

In the first attempt the configuration with both springs 30 mm length has been considered, as shown in Fig. 4. Activating the closure spring the system reaches the configuration in correspondence of the intersection between blue and green line. Afterwards, activating the opening spring the system reaches the configuration point in correspondence of the intersection between black and grey line. The main problem of this system is that during cooling, the springs do not stay in that configuration and change their values of elastic constant, so the system comes back to its original position. In the proper design condition the prototype after warming reaches the equilibrium configuration and only after the successive warming the system could change his configuration. The next challenge has been the definition of the suitable clearance between the springs. In fact, the closure spring has been configured to start from the compressed length (34 mm), while the antagonist spring has been set to his expanded length. In this way the problem of the elastic spring back has been solved. On the other side another problem arose, connected to the strength offered by the spring during the cold compression. In fact the force necessary for the cold compression of the spring with 15 turns and average diameter of 7.6 mm has been measured about 1N. To ensure the antagonist spring to be compressed by the closure spring during the activation of the system it has been manufactured in a way that in the point highlighted by a red circle in Fig. 5 where the opening spring starts to explicate the force, the closure spring performs a force about 3N, greater than minimum required (1N). The equilibrium conditions, opening and closure, are illustrated in Fig. 5.

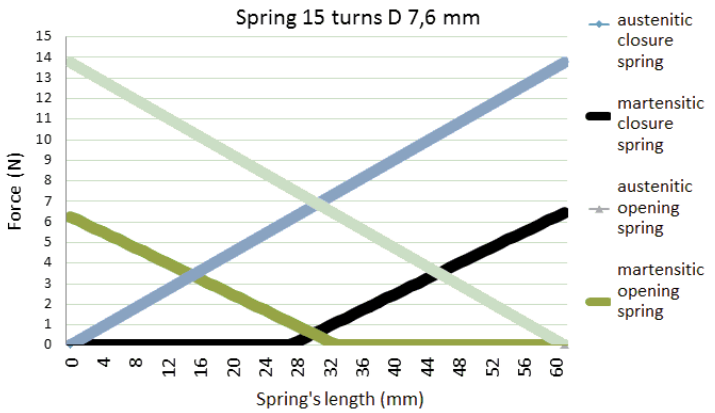

Fig. 4. Force – Spring's length diagram in the first experiment.

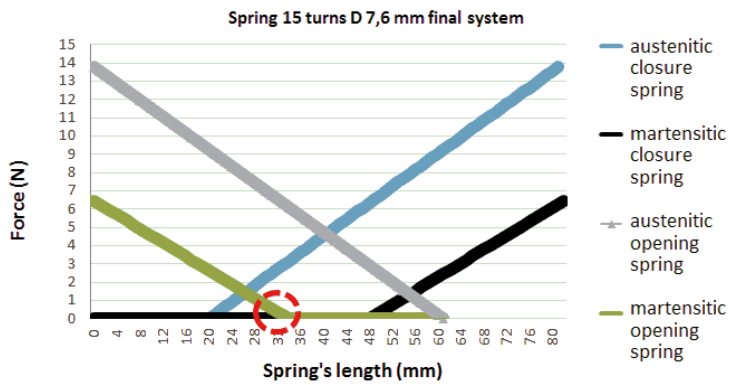

Fig. 5. Force – Spring's length diagram in the final configuration.

Such system allows a total stroke of 14 mm and fully solves the problems relative to the elastic return and the strength offered by antagonist spring during the cold compression. The hole of the prototype has been realized with a diameter of 11 mm. It is important to highlight how in this sliding variable aperture, the profile is manufactured with a circular aperture because the non-circular profile created by the aperture discussed allowed less radiation access into the cavity when compared to a circular aperture of the same area. This fact may be ascribed to the incident solar radiation which shows a circular Gaussian distribution as reported by Al Hamidi et al. (2011). Fig. 6 shows the entire prototype realized in the laboratory in a total aperture configuration: the power source system has been configured in series connection so that the activation of opening and closure system can be performed employing only one power supply. To achieve a variable aperture it was important to analyze different values of voltage (and consequently current) to be applied by means of the power supply which allows a partial stroke compared to the total stroke (14 mm). The purpose has been achieved with the identification of the voltage necessary to obtain different partial aperture. Starting from the closure configuration, it has been measured the value of length reach by each couple of spring during 5 s of activation of the aperture spring. After the activation of the SMA, the system stays on the position. Finally in Fig. 7 the map of the position of the actuators starting from a closure configuration is reported as a function of the applied voltage.

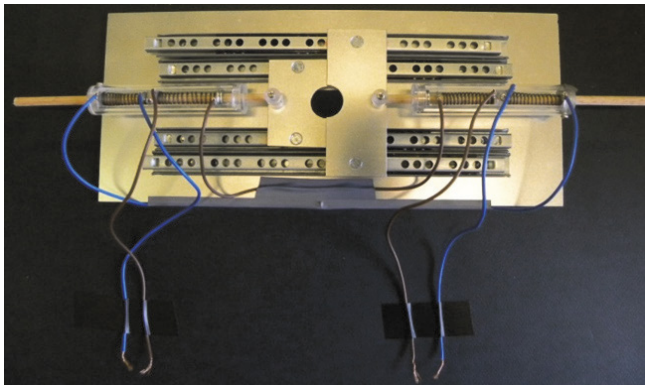

Fig. 6. The prototype.

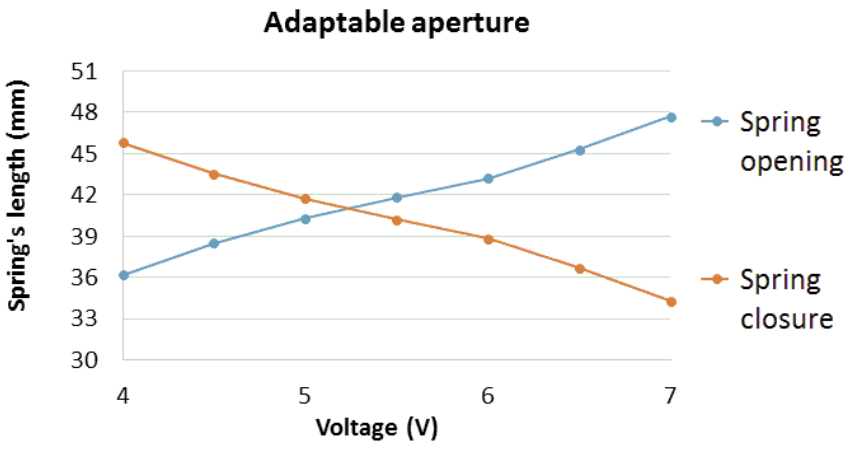

Fig. 7. Diagram Length – Voltage for the final configuration.

As evidenced from the Fig. 7 the behavior of the SMA's spring is not linear. For instance, activating the opening spring with a voltage of 5.4 V, the system reaches the configuration shown in Fig. 8 with the spring's length reported in Fig. 7. Current values required for the full activation of the system are comprised between 4.3 and 5.3 A.

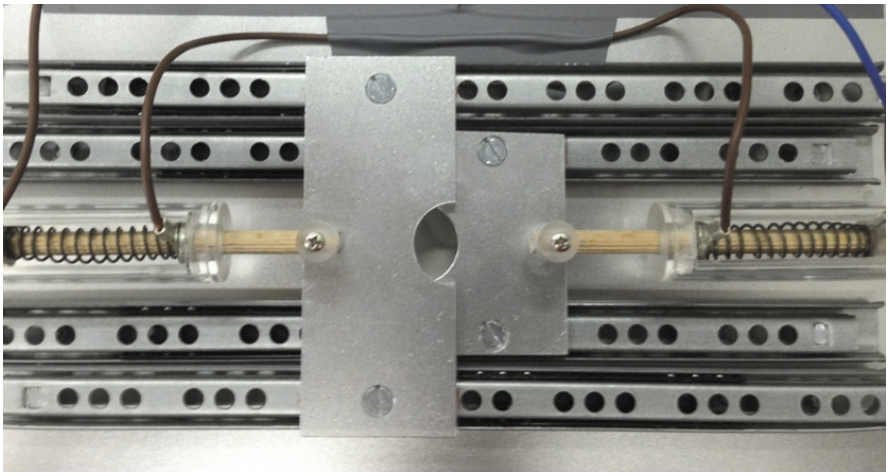

Fig. 8. The prototype in a partially closed position.

4. Conclusions

The main goal of this work has been the design and manufacturing of a prototypal actuator system by means of shape memory alloys elements with modular stroke. The developed prototypal system has been used to analyze the working principle and its performance in terms of response and positioning with particular reference to the stroke. The activation, both in opening and closure condition, is by Joule effect. In the experimental set-up each cylinder holds two shape memory alloy springs, employed to replace the electromechanical actuators. The design and the characterization of the actuation system itself can be simplified and in addition different values of aperture can be obtained according to different values of applied voltage alternatively to the opening and closure spring, realizing a variable aperture. One of the main innovations of the prototype is the possibility to calibrate the right aperture depending on the value of irradiance just by acting on the SMA opening and closure springs. By changing the applied voltage on the opening and closure spring is possible to set the optimum aperture, overcoming the limitation of the combination SMA-steel spring.

The spring 6.6 mm average diameter, compared to the springs 7.6 mm average diameter and the same number of turns, gives more force but at the same time allows a lower stroke. In the comparison between springs with the same diameter, the spring with 13 turns shows a force practically equal to the spring with 15 turns but experimentally smaller stroke has been measured. Anyway, to satisfy our purpose to maximize the stroke realized by the actuator, it has been observed that the spring with 15 turns and 7.6 mm diameter can be considered the optimal solution. To achieve a right operation mode of the prototype friction has been reduced and a satisfactory alignment conditions among different parts achieved.

References

Al Hamidi, Y., Abdulla, S., El Zamli, M., Rizk, I., Ozalp, N., 2011. Design, manufacturing and testing of an aperture mechanism for a solar reactor. In: Proceedings of the ASME 5th International Conference on Energy Sustainability, Washington DC, USA, 1661-1672.

Besarati, S.M., Yogi Goswami, D., Stefanakos, E.K., 2014. Optimal heliostat aiming strategy for uniform distribution of heat flux on the receiver of a solar power tower plant. Energy Conversion and Management 84, 234-244.

Boschetto A., Bottini L., Costanza G., Tata M.E., 2019. Shape memory activated self-deployable solar sails: small-scale prototypes manufacturing and planarity analysis by 3D laser scanner. Actuators, 8 (2), 38.

Costanza G., Tata M.E, 2018. A novel methodology for solar sail opening employing shape memory alloy elements. Journal of intelligent materials systems and structures, 29 (9), 1793-1798.

Costanza G., Leoncini G., Quadrini F., Tata M.E., 2017. Design and characterization of a small-scale solar sail prototype by integrating NiTi SMA and carbon fiber composite. Advances in materials science and engineering, 2017, article number 8467971.

Costanza G., Tata M.E., Libertini R., 2016. Effect of temperature on the mechanical behavior of Ni-Ti Shape Memory Sheets. In TMS 2016: 145th Annual Meeting & Exhibition: Supplemental Proceedings, Nashville, TN, USA, 433-439.

Costanza, G., Paoloni, S. Tata, M.E., 2014. IR thermography and resistivity investigations on Ni-Ti shape memory alloys. Key Engineering Materials 605, 23-26.

Costanza, G., Tata, M.E., Calisti, C., 2010. Nitinol one way shape memory springs: thermomechanical characterization and actuator design. Sensors and Actuators A, Physical, 157 (1), 113-117.

Hathaway, B.J., Chandran, R.B., Sedler, S., Thomas, D., Gladen, A., Chase, T., Davidson J.H. 2016. Effect of flow rates on operation of a solar thermochemical reactor for splitting CO_2 via the isothermal ceria redox cycle. Journal of solar energy engineering 138 (1), Article number 011007.

Kräupl S., Frommherz U., Wieckert C., 2006. Solar carbotermic reduction of ZnO in a two-cavity reactor: laboratory experiments for a reactor scale up. Journal of solar energy engineering 128 (1), 8-15.

Ophoff C., Korotunov S., Ozalp N., 2017. Optimization of design and process parameters for maximized and stable solar receiver efficiency. In: Proceedings of 2nd Thermal and Fluids Engineering conference, Las Vegas, NV, USA, 1263-1279.

Wang, Z., Zu, X., Feng, X., Dai, J., 2002. Effect of thermomechanical treatment on the two-way shape memory effect of niTi alloy Springs. Materials Letters 54 (1), 55-61.

Z'Graggen A., Haueter, P., Trommer, D., Romero, M., De Jesus, J.C., Steinfeld, A., 2006. Hydrogen production by steam-gasification of petroleum coke using concentrated solar power-II Reactor design, testing and modeling. International journal of hydrogen energy 31 (6), 797-811.